

Vibronic dynamics in electron continuum - iterative solvers

Martina Čosićová,^{*} Jan Dvořák,[†] and Martin Čížek[‡]

Charles University, Faculty of Mathematics and Physics, Institute of Theoretical Physics,
V Holešovičkách 2, 180 00 Prague, Czech Republic

(Dated: July 26, 2023)

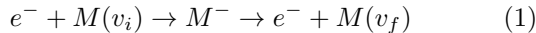
We present a general two-dimensional model of conical intersection between metastable states that are vibronically coupled not only directly but also indirectly through a virtual electron in the autodetachment continuum. This model is used as a test ground for design and comparison of iterative solvers for resonance dynamics in low-energy electron-molecule collisions. Two Krylov-subspace methods with various preconditioning schemes are compared. To demonstrate the applicability of the proposed methods on even larger models, we also test the performance of one of the methods on a recent model of vibrational excitation of CO₂ by electron impact based on three vibronically-coupled discrete states in continuum (Renner-Teller doublet of shape resonances coupled to sigma virtual state) including four vibrational degrees of freedom. Two-dimensional electron energy-loss spectra resulting from the electron-molecule scattering within the models are briefly discussed.

Keywords: Schrödinger equation, Krylov subspace iterative methods, vibronic coupling.

I. INTRODUCTION

Despite of a long history of investigations [1–3], the collisions of low-energy electrons with molecules still represent a fascinating and challenging field of study. By low energy we mean here the energy below the electronic-excitation threshold, i. e. the energy that does not exceed few units of electron volt. Even these low energies lead to many interesting phenomena like appearance of sharp structures in cross sections [4, 5] or the possibility to select dissociation into different anionic fragments by tuning the energy [6, 7]. This topic is both interesting for practical applications [8] and challenging for the theory even for small polyatomic molecules [9–15].

In this paper we will focus on the process of the vibrational excitation in collision of an electron e^- with a molecule M initially in a vibrational state $|v_i\rangle$

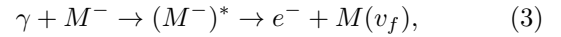


mediated by one or several metastable anion states M^- . After the process, the molecule is left in a final vibrational state $|v_f\rangle$. The total energy E during the collision is conserved

$$E = \epsilon_i + E_{v_i} = \epsilon_f + E_{v_f}, \quad (2)$$

where ϵ are electron energies and E_v energies of vibrational states of the molecule for the initial and the final states, before and after the collision. This process is closely related to the process of photodetachment of an

electron e^- from a molecular anion M^-



with initial energy E of the system defined now by the energy of the photon γ shone on the anion to excite it to the state $(M^-)^*$. The dynamics of both of these processes is driven by potential energy states of the negative molecular ion and their widths for decay into electronic continuum channels [16]. The energies of the released electrons are sensitive to the relative position of the anion and the neutral molecular states and the selection rules are different than for the radiative transitions [17–19].

The goal of this paper is to advance the detailed theory of the dynamics of the electron detachment from anions in such processes. In the development of the theoretical methods, we keep in mind the description of experiments that study in detail the energies of released electrons [16, 20, 21], and in particular, we calculate the two-dimensional electron energy-loss spectrum (2D EELS) for our model. The 2D electron loss spectroscopy was pioneered by Currel and Commer [22, 23] and further developed by Allan and collaborators [24]. Up to now, a dozen of high-resolution spectra for different molecules have been measured [16, 24–31] but the detailed understanding of such spectra for polyatomic molecules is mostly lacking.

In this paper, we present and test a general scheme for solving the nuclear dynamics of the negative ion formed in the collision of an electron with a polyatomic molecule. The scheme is tailored for a class of models that are inspired by the pseudo-Jahn-Teller model of Estrada, Cederbaum and Domcke [32] with modifications meant to make it a more realistic model of real molecules. This approach combines a model of vibronic coupling of several anionic states expanded in low-order polynomials in vibrational coordinates close to equilibrium geometry of the neutral molecule with projection-operator approach to include the interaction of the anion discrete states with the electronic continuum. The model is rather flexible in

^{*} Current affiliation: Department of Applied Mathematics, Faculty of Electrical Engineering and Computer Science, VŠB – Technical University of Ostrava, Czech Republic

[†] Current affiliation: Chemical Sciences Division, Lawrence Berkeley National Laboratory, One Cyclotron Road, Berkeley, California 94720, USA

[‡] Martin.Cizek@mff.cuni.cz

adding states and vibrational degrees of freedom and the present scheme has been used to produce the results in our previous work on CO₂ [33–35]. In these papers we did not explain the methods and their performance in detail, a gap that is meant to be filled by this work.

We start Section II by reviewing the projection-operator approach to the dynamics of vibrational excitation in electron collisions with molecules. We then proceed by reminding the model of Estrada et al. [32] and propose its generalization by including the vibronic coupling through the electron continuum in addition to the direct vibronic coupling present in the original model. This section is concluded by explaining the representation of the wave-function components and the Hamiltonian in a basis constructed from neutral vibrational states. In Section III, we first introduce the used iteration methods and preconditioning schemes and then we discuss their performance for the models. The section IV is devoted to a brief description of the obtained 2D spectra for the models and we conclude by summarising the results in Section V.

II. THEORY

The vibrational and resonance dynamics in electron-molecule collisions has been studied theoretically for a long time (see, for example, one of the review papers [2, 36–38]). The direct brute-force approach is only tractable for small molecules [39] or for small deformations [40]. Number of approximate schemes have therefore been developed: Born approximation, adiabatic-nuclei approximation, zero/effective range or semi-classical approaches. In the present work we focus on the development of the numerical schemes for the projection-operator approach based on the existence of an intermediate anion state (or states) that is responsible for the coupling of the electronic and vibrational motion. The approach is often used in its approximate form — the local complex potential approximation, but it is known to fail in predicting interesting phenomena like Wigner cusps or vibrationally excited Feshbach resonances. The nonlocal approach is well developed for diatomic molecules [37, 41] but the attempts to use it for polyatomic molecules are scarce (see for example [42]). In addition to bringing more degrees of freedom, the polyatomic molecules also exhibit interesting features like vibronic coupling of resonances, conical intersections and exceptional points [43, 44]. Here, we follow the work of Estrada, Cederbaum and Domcke [32] (ECD86) and extend it to more general form of model functions and vibronic coupling. We start by presenting basic formulas resulting from the projection-operator formalism (see [37] for the comprehensive review of the approach). Then, we narrow the model to two vibrational degrees of freedom and two vibronically coupled discrete states.

A. Nonlocal model for multiple discrete states in continuum

The main idea of the nonlocal-discrete-state in continuum model is the assumption that the coupling of the electronic and vibrational degrees of freedom in the electron-molecule collision is mediated by one or a few discrete states and after their removal from the electronic continuum using projection-operator formalism of Feshbach [45], the electronic basis consisting of the discrete states and the orthogonalized continuum is diabatic. The vibrational excitation or dissociative attachment then proceeds through capture into the discrete state.

We define the projection operator

$$\mathcal{Q} = \sum_d |d\rangle\langle d|. \quad (4)$$

as a sum over a set of discrete states $|d\rangle$ and the complementary operator

$$\mathcal{P} = I - \mathcal{Q} \quad (5)$$

projecting on the background continuum. The basis in the background part can be chosen as the states that solve the background scattering problem

$$\mathcal{P}\mathcal{H}_{el}\mathcal{P}|\Phi_0, \epsilon\mu\rangle = (V_0 + \epsilon)|\Phi_0, \epsilon\mu\rangle. \quad (6)$$

Here, $V_0(\vec{q})$ is the potential energy surface of the neutral molecule, i. e. the energy of the ground electronic state $|\Phi_0\rangle$ as function of the positions of the nuclei \vec{q} . Since we consider only low-energy electron scattering below threshold for the electronic excitation of the molecule, the state Φ_0 is fixed and we will further omit it from the notation. The electron continuum states $|\epsilon\mu\rangle$ are thus uniquely described by the electron energy ϵ and some other quantum numbers collectively denoted by μ (typically angular momentum). All states $|d\rangle$ and $|\epsilon\mu\rangle$ thus form an orthogonal basis:

$$\langle d|d'\rangle = \delta_{dd'}, \quad (7)$$

$$\langle d|\epsilon\mu\rangle = 0, \quad (8)$$

$$\langle \epsilon\mu|\epsilon'\mu'\rangle = \delta_{\mu\mu'}\delta(\epsilon - \epsilon'). \quad (9)$$

The electronic Hamiltonian in the \mathcal{Q} -space is described by a matrix

$$\langle d|\mathcal{H}_{el}|d'\rangle = V_0\delta_{dd'} + U_{dd'} \quad (10)$$

where all matrix elements depend on the molecular geometry, i. e. positions of nuclei \vec{q} . The diagonal elements $V_d(\vec{q}) = V_0(\vec{q}) + U_{dd}(\vec{q})$ represent the diabatic discrete-state potentials and the off-diagonal part $U_{dd'}(\vec{q})$ the direct vibronic coupling among the states. The coupling between the discrete state $|d\rangle$ and the continuum $|\epsilon\mu\rangle$ is described by the coupling elements

$$\langle d|\mathcal{H}_{el}|\epsilon\mu\rangle = V_{de}^\mu(\vec{q}). \quad (11)$$

These elements represent the vibronic coupling¹ of the discrete state to the continuum and they also lead to the second order vibronic coupling among the discrete states mediated by continuum as described below.

This way, we parameterized the matrix elements given by Eqns. (6), (10), (11) of the Hamiltonian \mathcal{H}_{el} for the electron scattering from the molecule for each fixed position of the nuclei \vec{q} by functions $V_0(\vec{q})$, $U_{dd'}(\vec{q})$ and $V_{de}^\mu(\vec{q})$. To describe the electron scattering from the molecule including the vibronic dynamics, we start from the definition of the vibrational states $|v\rangle$ of the target neutral molecule:

$$H_0|v\rangle = (T_N + V_0)|v\rangle = E_v|v\rangle, \quad (12)$$

where T_N is the kinetic-energy operator for the nuclei and v is a set of quantum numbers that uniquely determine the vibrational states with energy E_v . It can be shown (see for example [37]) that the vibronic motion of the anion is described by the effective Hamiltonian

$$H_{ef} = H_0 + U + F, \quad (13)$$

which is the matrix in the indices d, d' and the operator in the space of vibrational degrees of freedom. In the equation above, H_0 is the Hamiltonian operator for the vibrations of the molecule multiplied by unity matrix $\delta_{dd'}$ in the discrete state indices, U is the matrix with the elements $U_{dd'}$ defined above and the operator F describes the dynamical coupling of the discrete-state space to the electronic continuum

$$F_{dd'}(E-H_0) = \sum_{\mu} \int_0^{\infty} V_{de}^\mu(\vec{q}) [E-H_0-\epsilon+i\eta]^{-1} V_{d'e}^\mu(\vec{q}') d\epsilon, \quad (14)$$

where η is a positive infinitesimal. This operator is a matrix in the discrete-state indices and nonlocal operator in the nuclear coordinate \vec{q} .

The discrete-state contribution to the T -matrix for vibrational excitation by electron scattering in a continuum state $|\epsilon_i\mu_i\rangle$ from the initial vibrational state v_i to final state v_f and leaving in continuum state $|\epsilon_f\mu_f\rangle$ is given by [32]

$$T_{\mu_f v_f \leftarrow \mu_i v_i} = \sum_{dd'} \langle v_f | V_{d\epsilon_f}^{\mu_f} [E - H_{ef}]_{dd'}^{-1} V_{d'\epsilon_i}^{\mu_i} | v_i \rangle \quad (15)$$

and is closely related to the integral cross section for the vibrational excitation event

$$\sigma_{v_f \leftarrow v_i} = \frac{2\pi^3}{\epsilon_i} \sum_{\mu_i \mu_f} |T_{\mu_f v_f \leftarrow \mu_i v_i}|^2. \quad (16)$$

¹ Note that we consider V_{de}^μ to be real quantities. This is a reasonable assumption since the coupling can be made real for a single \vec{q} by phase conventions and the dependence on \vec{q} is supposed to be weak (adiabaticity of the basis).

Finally, to simulate the full 2D electron energy-loss spectra, we have to collect vibrational excitation cross sections for all accessible final states

$$S(\epsilon_i, \Delta\epsilon) = \sum_{v_f} \sigma_{v_f \leftarrow v_i}(\epsilon_i) \rho(\Delta\epsilon - \Delta\epsilon_{v_f}), \quad (17)$$

where $\rho(\epsilon)$ is the resolution function of the spectrometer (simulated here with a Gaussian function with full width at half maximum equaled to 10 meV, which is comparable to the values in the experiment [24]). The energy loss $\Delta\epsilon_{v_f} = E_{v_f} - E_{v_i} = \epsilon_i - \epsilon_f$ in each term in Eq. (17) is fixed by the energy conservation. The function $S(\epsilon_i, \Delta\epsilon)$ gives the full experimental information in the electron energy-loss spectroscopy except for the angular resolution that can also be included [35] but it is not of the interest in the present paper.

B. Pseudo Jahn-Teller model of Estrada et al.

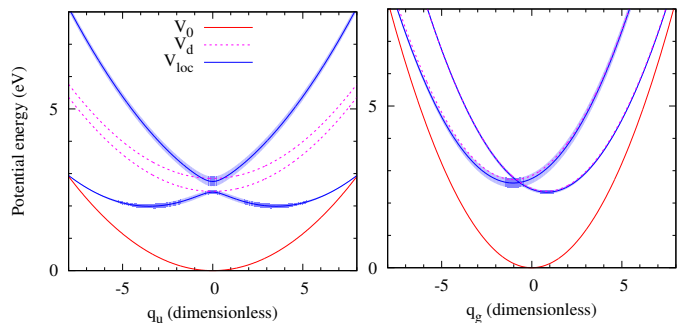


FIG. 1. Sections through the model potential energy surfaces in the $q_g = 0$ (left) and $q_u = 0$ (right) planes for the ECD86 model. Blue-shaded areas give the position and the width of the fixed nuclei electronic resonance.

Model by Estrada, Cederbaum and Domcke [32] assumes a molecule with an Abelian group of symmetry.

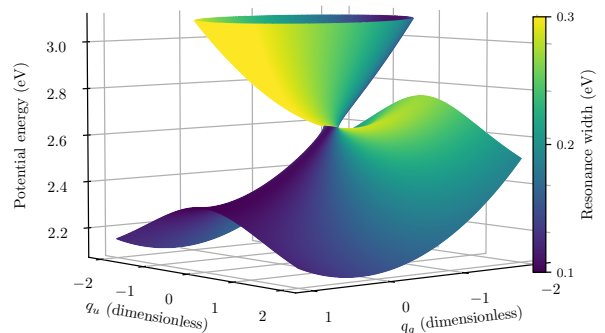


FIG. 2. Perspective view of the potential energy manifold for the ECD86 model. The width (inverse lifetime) is marked by the color scale.

They consider two discrete states $d = 1, 2$ that transform according to different irreducible representations of the symmetry group and are coupled vibronically through a nontotally symmetric vibrational mode q_u . They also consider excitation of another, totally symmetric mode q_g , so that the geometry of the molecule within the model is describe by a vector $\vec{q} = (q_g, q_u)$. The symmetry then dictates the structure of the matrix U :

$$U = \begin{pmatrix} E_1 + \kappa_1 q_g & \lambda q_u \\ \lambda q_u & E_2 + \kappa_2 q_g \end{pmatrix}. \quad (18)$$

This is a completely general form of the dependence of the matrix U on coordinates when the terms are restricted up to the first order in \vec{q} and the symmetry requirements are taken into account. Similarly, we can expand the matrix of the discrete-state-continuum coupling. For simplicity, we consider only two partial waves $|\epsilon\mu\rangle$ for $\mu = e, o$ representing one even and one odd linear combination of partial waves coupled to the discrete-state space. In principle, we could consider more partial waves but they could be decoupled from the problem by a unitary transformation, grouping thus partial waves into effective channels with number of channels not exceeding the dimension of the \mathcal{Q} -space [46]. Estrada et al [32] considered the coupling matrix V_{de}^μ independent of the nuclear coordinates (we are going to lift this restriction in the next section). The symmetry selection rules then forbid the coupling V_{de}^μ to the different symmetry of the discrete state d and the partial wave μ . We therefore assume that the discrete state $d = 1$ has even symmetry as the $\mu = e$ partial wave and $d = 2$ has the symmetry of the odd partial wave $\mu = o$. Using Eq. (14), we then see that only the diagonal matrix elements $F_{11}(\epsilon)$ and $F_{22}(\epsilon)$ of the level-shift operator are nonzero. They can be generated from their imaginary parts (widths)

$$\begin{aligned} \Gamma_{11}(\epsilon) &= -2 \text{Im} F_{11} = 2\pi |V_{1\epsilon}^e|^2, \\ \Gamma_{22}(\epsilon) &= -2 \text{Im} F_{22} = 2\pi |V_{2\epsilon}^o|^2 \end{aligned}$$

by means of the integral transform $\mathcal{F}[\Gamma_{ii}(\epsilon)/2\pi]$ defined as (compare Eq. (14))

$$\mathcal{F}[f(\epsilon)] = \int \frac{f(x)}{\epsilon - x + i\eta} dx. \quad (19)$$

TABLE I. The values of the parameters describing the pseudo Jahn-Teller model of Estrada et al. [32].

Parameter	Value	Parameter	Value
ω_g	0.258	ω_u	0.091
E_1	2.45	E_2	2.85
κ_1	-0.212	κ_2	0.254
λ	0.318		
a_1	0.086	a_2	0.186
b_1	0.833	b_2	0.375
l_1	2	l_2	1

This transform can be worked out analytically for the assumed form of the widths

$$\Gamma_{dd}(\epsilon) = a_d \epsilon^{l_d+1/2} \exp(-b_d \epsilon) \quad (20)$$

(see [47]). To complete the model description we must give the vibrational Hamiltonian H_0 of the neutral molecule. The model assumes simply harmonic vibrations

$$H_0 = T_N + V_0 = -\frac{1}{2}\omega_g \frac{\partial^2}{\partial q_g^2} - \frac{1}{2}\omega_u \frac{\partial^2}{\partial q_u^2} + \frac{1}{2}\omega_g q_g^2 + \frac{1}{2}\omega_u q_u^2. \quad (21)$$

The vibrational eigenstates $|v\rangle$ satisfying Eq. (12) with this harmonic Hamiltonian can be numbered by two quantum numbers $\nu = (n_g, n_u)$ and the vibrational energies are given by standard harmonic oscillator formula $E_\nu = \omega_g(n_g + \frac{1}{2}) + \omega_u(n_u + \frac{1}{2})$.

The numerical values of ω_i and the parameters defining direct coupling matrix U and discrete-state-continuum matrix V_e for the model studied in [32] and used here for testing are given in Table I. Note that several variants of the model were studied in [32]. Here we study only the most complex form of the model with the values of parameters as given in the table. To visualize the character of the model, we show the one dimensional sections through the model potentials in Fig. 1. The functions shown are $V_0(\vec{q})$, $V_d(\vec{q}) = V_0(\vec{q}) + U_{dd}(\vec{q})$ and the local complex potential $V_{loc}(\vec{q})$. The last function is defined as the position $V_{loc} = E_R - \frac{i}{2}\Gamma_R$ of the pole of the fixed nuclei S matrix, which has to be located iteratively [34]. The perspective view of the local complex potential $\text{Re} V_{loc}$ colored by values of $-2 \text{Im} V_{loc}$ is also shown in Fig. 2.

C. Generalized model with vibronic coupling with continuum states

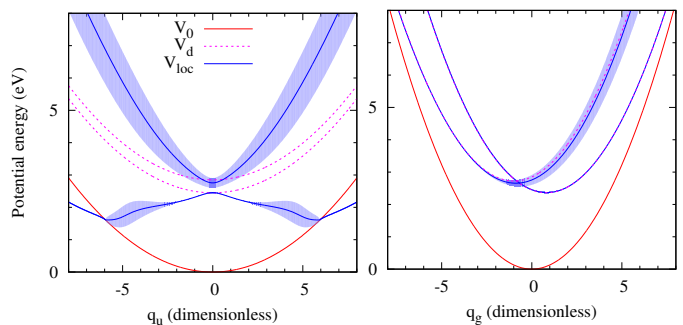


FIG. 3. Sections through the model potentials in the $q_g = 0$ (left) and $q_u = 0$ (right) planes for the new model.

The vibronic model above assumes the most simple structure of the discrete-state-continuum coupling matrix $V_\epsilon = \{V_{de}^\mu\}$ with row index d and column index μ :

$$V_\epsilon = \begin{pmatrix} V_{1\epsilon}^e(\vec{q}) & V_{1\epsilon}^o(\vec{q}) \\ V_{2\epsilon}^e(\vec{q}) & V_{2\epsilon}^o(\vec{q}) \end{pmatrix} = \begin{pmatrix} \sqrt{\Gamma_{11}/2\pi} & 0 \\ 0 & \sqrt{\Gamma_{22}/2\pi} \end{pmatrix}.$$

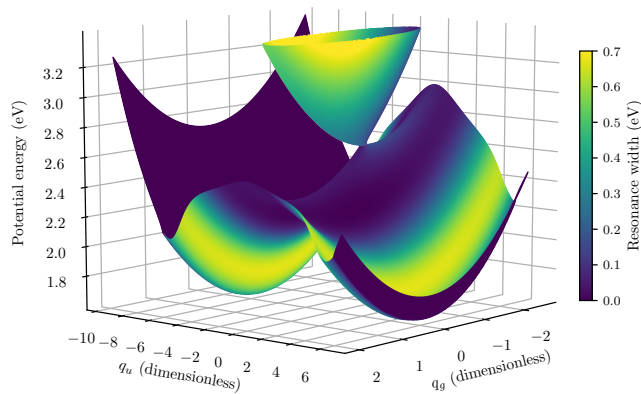


FIG. 4. Perspective view of the potential energy manifold for the new model, colored by the width of the resonance.

Here, we would like to go one step beyond the approximation of the coupling matrix by constant terms and we expand the matrix to the first order in the normal vibrational coordinates. This generalization is very useful in the description of the interaction of resonances through the electronic continuum that is switched off in the equilibrium geometry, but becomes nonzero with deformation as, for example, in pyrrole molecule [48]. This feature was also important ingredient of the model for CO₂ molecule [33, 34]. We will further assume that the dependence of $V_{de}(\vec{q})$ on the electron energy ϵ and the normal coordinates is separable. Taking into account the symmetry of the system, we get

$$V_\epsilon = \begin{pmatrix} f_1^e(\epsilon)[1 + \lambda_1 q_g] & f_1^o(\epsilon)q_u \\ f_2^e(\epsilon)q_u & f_2^o(\epsilon)[1 + \lambda_2 q_g] \end{pmatrix},$$

where the terms that couple a discrete state to the partial wave of different symmetry must be odd functions of q_u . We see that half of the total number of 12 terms (up to first order in \vec{q}) in the coupling matrix are zero due to the symmetry. For the purposes of the testing of the numerical methods, we choose the same form of the energy dependence as in the original model:

$$2\pi|f_d^\mu|^2 = a_d^\mu \epsilon^{l_d^\mu + 1/2} \exp(-b_d^\mu \epsilon) \quad (22)$$

with the values of the parameters given in Table II.

TABLE II. The values of the parameters describing the generalization of the model.

Parameter	Value	Parameter	Value
a_1^e	0.07	a_2^e	0.1
b_1^e	0.25	b_2^e	0.5
l_1^e	0	l_2^e	0
a_1^o	0.186	a_2^o	0.15
b_1^o	0.375	b_2^o	0.8
l_1^o	1	l_2^o	1
λ_1	0.2	λ_2	0.1

Using formula (14), we see that the structure of the nonlocal level-shift operator $F(E - H_0)$ is much richer:

$$\begin{aligned} F_{11} &= (1 + \lambda_1 q_g) \mathcal{F}[f_1^e f_1^e] (1 + \lambda_1 q_g) + q_u \mathcal{F}[f_1^o f_1^o] q_u, \\ F_{22} &= q_u \mathcal{F}[f_2^e f_2^e] q_u + (1 + \lambda_2 q_g) \mathcal{F}[f_2^o f_2^o] (1 + \lambda_2 q_g), \\ F_{12} &= (1 + \lambda_1 q_g) \mathcal{F}[f_1^e f_2^e] q_u + q_u \mathcal{F}[f_1^o f_2^o] (1 + \lambda_2 q_g), \\ F_{21} &= q_u \mathcal{F}[f_1^e f_2^e] (1 + \lambda_1 q_g) + (1 + \lambda_2 q_g) \mathcal{F}[f_1^o f_2^o] q_u, \end{aligned} \quad (23)$$

where we used the integral transform (19) again. The ordering of the terms that depend on q_i with respect to $\mathcal{F}(\epsilon)$ must be kept because we substitute the operator $\epsilon = E - H_0$, which does not commute with the normal coordinates.

The potentials for the new generalized model are visualised in Figs. 3 and 4. Note that the structure of such conical intersections in continuum have been investigated in [43, 44]. In accordance with their findings the potential manifolds shown in Figs. 2 and 4 do not intersect in a single point like regular conical intersections but in a line segment bounded by two exceptional points. The form of our model as given by Eq. (23) is more general than the expansion investigated in [43, 44] because they studied a linear coordinate expansion of the width function Γ whereas we prescribe the linear expansion of the coupling matrix V_ϵ , which is more natural for the subsequent treatment of the dynamics. In our case, the linear form of the coupling matrix produces also quadratic terms in widths in Eq. (23). When the quadratic terms are omitted, we recover the form used in [43, 44]. However, we can not omit these terms in the dynamics since it would distort the unitarity of the S matrix.

D. Numerical representation of the dynamics

For the numerical solution of the dynamics, we expand wave-function components in the harmonic oscillator basis $|v\rangle = |n_g, n_u\rangle$ associated with the model Hamiltonian of the neutral molecule (21). We first rewrite Eqs. (15), (16) for the cross section as

$$\sigma_{v_f \leftarrow v_i} = \frac{2\pi^3}{\epsilon_i} \sum_{\mu_i \mu_f} |\langle \Phi_{v_f}^{\mu_f} | \Psi_{v_i}^{\mu_i} \rangle|^2, \quad (24)$$

where we defined auxiliary wave-functions $|\Phi_v^\mu\rangle$ with components

$$\Phi_{d, n_g, n_u}^{v\mu} = \langle n_g, n_u | V_{de}^\mu | v \rangle, \quad (25)$$

and with energy according to the conservation law (2), i. e. $\epsilon = E - E_v$. The anion wave function $|\Psi_{v_i}^{\mu_i}\rangle$ satisfies

$$(E - H_{ef}) |\Psi_{v_i}^{\mu_i}\rangle = |\Phi_{v_i}^{\mu_i}\rangle. \quad (26)$$

In the harmonic oscillator basis, this equation represents a system of linear equations for unknown components of the discrete-state wave function

$$\Psi_\alpha \equiv \Psi_{d, n_g, n_u} = \langle d | \langle n_g, n_u | \Psi_{v_i}^{\mu_i} \rangle, \quad (27)$$

where we introduced a compound index $\alpha \equiv (d, n_g, n_u)$. Using this notation the matrix of this system $A_{\alpha, \alpha'}$ reads

$$A_{\alpha, \alpha'} = \langle n_g, n_u | (E - H_{ef})_{dd'} | n'_g, n'_u \rangle \quad (28)$$

and the scalar product in Eq. (24) can be written as the sum $\sum_{\alpha} \equiv \sum_d \sum_{n_g} \sum_{n_u}$ over the components of $\Phi_{\alpha}^{v_f \mu_f}$ and Ψ_{α} . We cut of the basis in each dimension keeping the states $|n_g\rangle$ for $n_g = 0, 1, \dots, N_g - 1$ and $|n_u\rangle$ for $n_u = 0, 1, \dots, N_u - 1$. The states Ψ_{α} are thus represented by $N = 2N_g N_u$ component vectors and A is a $N \times N$ matrix.

For the solution of Eq. (26) in the original model, Estrada et al. [32] devised a specially tailored method based on the block-tridiagonal structure of the matrix A . Our aim in this paper is to develop a more general method capable of solving a larger class of models and test it both on the original model and on our generalization. The matrix A is large but sparse. From the character of the problem, it is also complex symmetric, but not Hermitian. The structure of the matrix A depends on the order of the basis vectors as illustrated in Fig. 5 for the generalized model.

III. KRYLOV-SUBSPACE ITERATION METHODS

The Krylov-subspace iteration methods are well suited for solving Eq. (26). The main idea of all of the Krylov-subspace methods is that they solve a linear system

$$Ax = b$$

iteratively producing a sequence $x_0, x_1, x_2, \dots, x_n$ of approximations of the solution vector x in the Krylov-subspace, i. e. in the space

$$\mathcal{K}_n(A; r_0) = \text{span} \{r_0, Ar_0, A^2 r_0, \dots, A^{n-1} r_0\}.$$

where $r_0 = b - Ax_0$ denotes the initial residual vector. The methods differ by the definition of the "ideal" approximation of the solution x_n within the Krylov subspace and usually proceed by application of simple recursive formulas. To produce the Krylov subspace we only need to implement the matrix multiplication Aw for an arbitrary vector w . The choice of the harmonic basis is very convenient for implementation of this matrix multiplication. From Eqs. (13), (18), (23), we can see that the multiplication by the matrix A can be decomposed to successive multiplications by energy-dependent diagonal factors, for example,

$$\begin{aligned} [(E - H_0)w]_{\alpha} &= (E - E_{n_g, n_u})w_{d, n_g, n_u}, \\ [\mathcal{F}(E - H_0)w]_{\alpha} &= \mathcal{F}(E - E_{n_g, n_u})w_{d, n_g, n_u}. \end{aligned}$$

and by operators of the coordinates q_g and q_u

$$\begin{aligned} [q_g w]_{\alpha} &= \frac{1}{\sqrt{2}} (w_{d, n_g - 1, n_u} \sqrt{n_g} + w_{d, n_g + 1, n_u} \sqrt{n_g + 1}) \\ [q_u w]_{\alpha} &= \frac{1}{\sqrt{2}} (w_{d, n_g, n_u - 1} \sqrt{n_u} + w_{d, n_g, n_u + 1} \sqrt{n_u + 1}). \end{aligned}$$

These operations can be implemented very efficiently. Note that all energy factors and square roots can be pre-calculated and stored before starting the iteration process. Compared to a matrix-vector multiplication, which requires $O(N^2)$ operations for full matrices, the above procedure requires only $O(N)$ operations (with the operation count being approximately three times larger for the generalized model due to more complicated structure of the operator F). The efficiency of the method of solution of Eq. (26) is then given by the rate of convergence of the sequence x_n to the solution, which is judged by monitoring the size of the norm of the residuum $\|r_n\| = \|b - Ax_n\|$. In the following tests we stop the iterations when the value $\|r_n\| < 10^{-6} \|b\|$ is reached.

A. Methods of interest

Saad and Schultz [49] developed the generalized minimal residual (GMRES) method, one of the most widely used Krylov-subspace methods. This method constructs an orthonormal basis v_1, v_2, \dots, v_n of the n -th Krylov subspace $\mathcal{K}_n(A; r_0)$ using the Arnoldi algorithm that can be written in the matrix form as

$$AV_n = V_{n+1} \tilde{H}_n, \quad V_n = [v_1 | v_2 | \dots | v_n]$$

, where $\tilde{H}_n \in \mathbb{C}^{(n+1) \times n}$ is an upper Hessenberg matrix. The approximation x_n of the solution in each step is given by the condition that the residual vector $r_n = b - Ax_n$ satisfies the optimality property:

$$\|r_n\| = \min_{x_n \in x_0 + \mathcal{K}_n(A; r_0)} \|b - Ax_n\|. \quad (29)$$

If we write $x_n = x_0 + V_n y_n$, this condition leads to the $(n+1) \times n$ least-square problem for y_n :

$$y_n = \arg \min_{y \in \mathbb{C}^n} \left\| \|r_0\| e_1 - \tilde{H}_n y \right\|,$$

which has to be solved in every iteration.

An advantage of the GMRES method is that it can be used for any matrix A with no other special properties required than the regularity. On the other hand, each new basis vector at every iteration step has to be orthogonalized to all previous vectors. Thus, the size of the matrix V_n grows during the iteration process and if the method does not converge quickly, the storage space and the time needed for each step grows significantly. Note that the matrix A of our system of equations is complex symmetric (i. e. not Hermitian). For this reason, the Conjugate gradient method (which, unlike the GMRES method, uses short-term recurrences to construct the basis of the Krylov subspace, making it much less computationally demanding) can not be used to solve it. It is known [50] that for non-normal matrices it is not possible to define an 'optimal' iterative process (i. e. a process that minimizes the residual or certain norm of the error over the Krylov subspace) that constructs the basis of Krylov

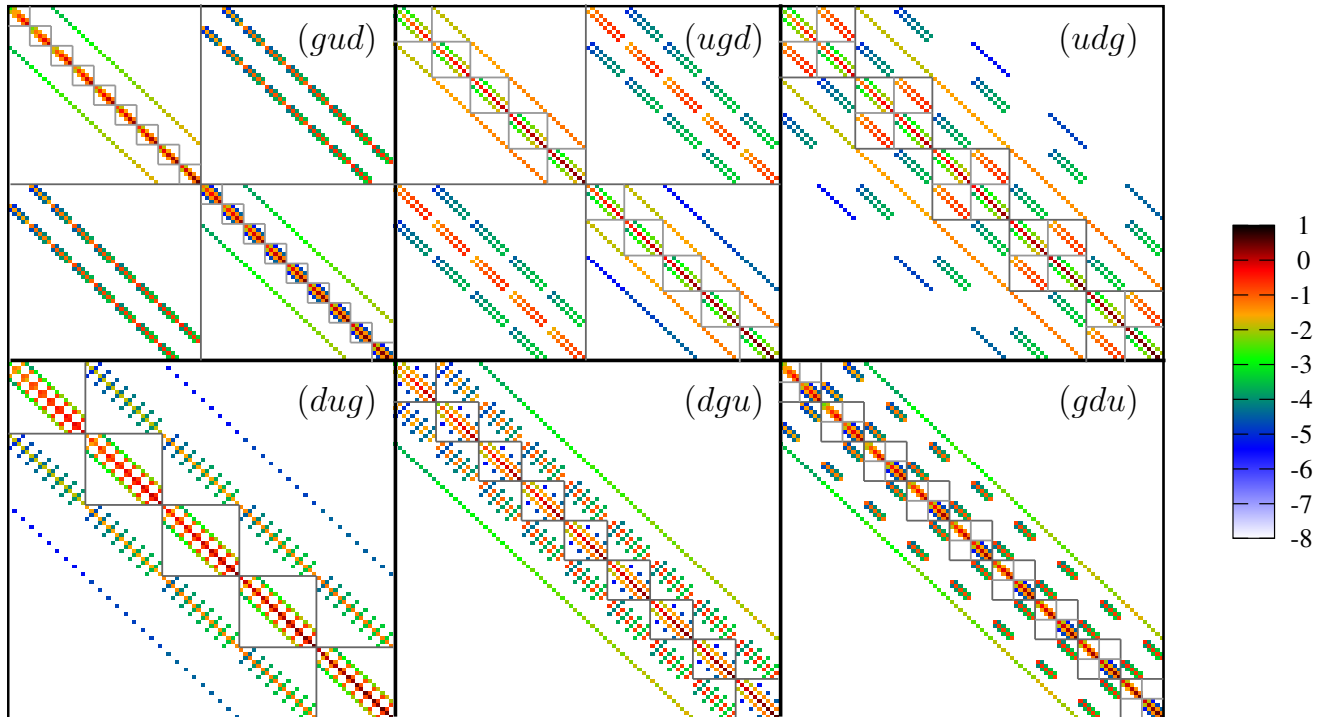


FIG. 5. Structure of the matrix A of the generalized model depending on the ordering of the basis, where the order is given by three letters d , g , and u representing the discrete states and vibrational modes q_g and q_u . The first index changes the fastest. The size of the matrix elements is represented by color in a logarithmic scale. The block-diagonal parts used for preconditioning are shown by the squares and for some orderings, the blocks corresponding to the discrete state are also indicated.

subspace using short-term recurrences [51]. For complex symmetric matrices van der Vorst and Mellisen [52] presented an alternative way to define an iterative process based on three-term recurrences and derived the conjugate orthogonal conjugate gradient (COCG) method. Setting $v_0 = r_0 = b - Ax_0$, the basis of the Krylov subspace is constructed using the recursive formula

$$v_{n+1} = Av_n + \alpha_n v_n + \beta_n v_{n-1},$$

where α_n and β_n follow from the conditions $\langle v_{n+1}|v_n \rangle_S = 0$ and $\langle v_{n+1}|v_{n-1} \rangle_S = 0$. These conditions are analogous to those that define the Conjugate gradient method, in which, however, we have replaced the standard scalar product with the symmetrized bilinear form

$$\langle a|b \rangle_S = \langle a^*|b \rangle, \quad a, b \in \mathbb{C}^N.$$

Note that the complex conjugation in the left argument cancels the complex conjugation in the standard definition of the scalar product. The bilinear form $\langle \cdot | \cdot \rangle_S$ is not therefore positive definite but it preserves the symmetry of the matrix A . This process ensures that vectors v_0, v_1, \dots, v_n satisfy the conjugate orthogonality property (vectors $a, b \in \mathbb{C}^N$ are conjugate orthogonal if

$\langle a|b \rangle_S = 0$). The whole iterative process is thus analogous to the conjugate gradient method but the convergence after N steps (N being the dimension of the matrix A) is not guaranteed in exact arithmetic. In addition, the iterations do not have to converge at all since the symmetrized product can be zero (or very small) even for nonzero vectors. In practice, however, the convergence is usually achieved. Moreover, (especially with proper preconditioning) it is often rather fast.

B. Preconditioning

In this paper, by preconditioning we understand the transformation of the original linear system $Ax = b$ into an equivalent problem (see, for example, [53])

$$M^{-1}AM^{-T}y = M^{-1}b, \quad \text{for } y = M^T x, \quad (30)$$

with a regular matrix M . This way, the preconditioning preserves the symmetry of the matrix A . As a rule of thumb, a good preconditioner M is represented by some fast invertible approximation of the original matrix A , but there are no exact guidelines for choosing the

ideal matrix M ensuring a fast convergence for the transformed problem. There is a large variety of preconditioners known in the literature but usually they are proposed for specific problems with matrices A having some special properties. We tested some of the preconditioning options but we found that the most simple methods work best for the present problem [54, 55]. In the following, we discuss different possibilities of block-diagonal preconditioning. For this choice we define the matrix M as a block diagonal section of the original matrix A . Depending on the structure of the blocks, the individual blocks can either be inverted directly to construct M^{-1} or a banded structure of the blocks can be used. The exact structure of the block depends on the ordering of the basis (see Fig. 5). We thus define three different preconditioners M^{dg} , M^{gu} , M^{du} with small diagonal blocks of the sizes $N_u \times N_u$, 2×2 and $N_g \times N_g$, respectively, and three preconditioners M^d , M^g , M^u with large blocks of sizes $N_g N_u \times N_g N_u$, $2N_u \times 2N_u$ and $2N_g \times 2N_g$. To be more specific, in the (dug) ordering of the basis functions, the small-block preconditioning matrix M^{ug} has $N_u N_g$ blocks $M^{(n_u, n_g)}$ of the size 2×2 with the matrix elements

$$M_{d,d'}^{(n_u, n_g)} = A_{(d, n_g, n_u), (d', n_g, n_u)} \quad (31)$$

and the large-block preconditioning matrix M^g has N_g blocks $M^{(n_g)}$ of the size $2N_u \times 2N_u$ with the matrix elements

$$M_{dn_u, d'n'_u}^{(n_g)} = A_{(d, n_g, n_u), (d', n_g, n'_u)}. \quad (32)$$

To apply the preconditioning we need to act with M^{-1} on a vector w with components w_{d, n_g, n_u} . This can be done block by block; for example, to apply the preconditioner M^u we invert each block $M^{(n_u)}$ using the LL^T (or LDL^T) decomposition and act on the section of w_{d, n_g, n_u} -vector for this fixed n_u

$$[M^{(n_u)^{-1}} w]_{d, n_g, n_u} = \sum_{d', n'_g} [M^{(n_u)^{-1}}]_{dn_g, d'n'_g} w_{d', n'_g, n_u}. \quad (33)$$

This is repeated for each n_u . Note that the inverting of the preconditioning matrices $M^{(n_u)}$ should be done just once and stored before starting iterations. Moreover, in practice the L (and D) matrix is stored in memory instead of $M^{(n_u)^{-1}}$.

C. Numerical testing

We applied the above described methods GMRES and COCG to solve the system (26) with the matrix (28) for the original ECD86 model and for our generalization of the model. The performance of each method for different preconditioning is discussed separately for the two models in the next two paragraphs. The last paragraph also discusses the performance of the COCG method for a realistic model that describes inelastic electron scattering from the CO_2 molecule.

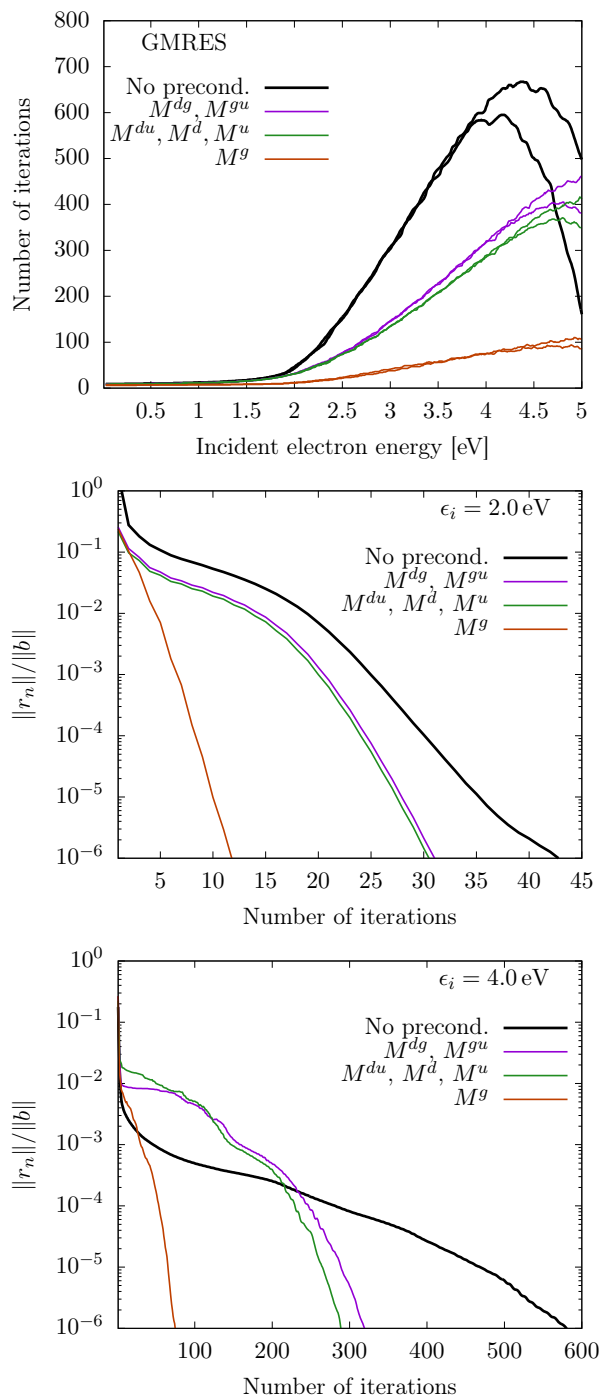


FIG. 6. Convergence of GMRES method for the model of Estrada et al. [32] for various preconditioners. Number of iterations needed for each electron energy (top) and convergence of residuum for $\epsilon_i = 2$ eV and 4 eV (bottom two panels). The top part shows results for both right-hand sides $\mu = e, o$ of the linear system; bottom two parts display just $\mu = e$.

a. Performance of the methods for ECD86 model is shown in Fig. 6 and Fig. 7. Each of the figures is devoted to one of the methods comparing different preconditioning schemes. The top graph summarises the number of

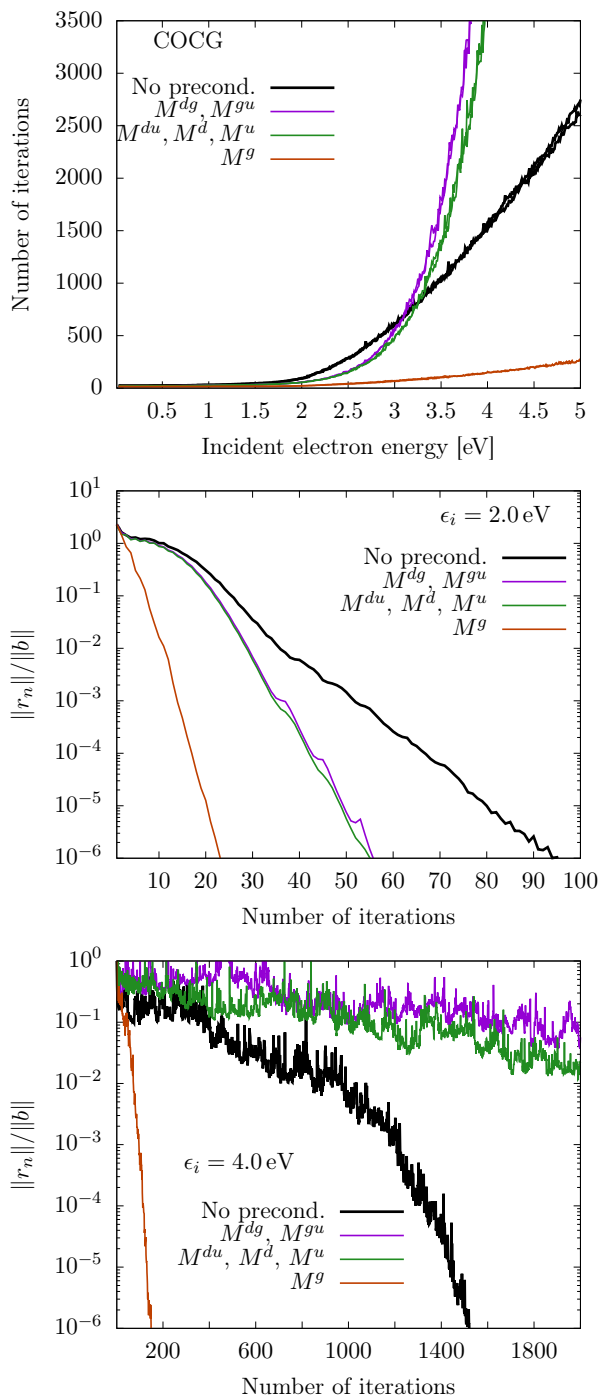


FIG. 7. Convergence of COCG method for the model of Estrada et al. [32], see also caption of Fig. 6 for details.

iterations needed for convergence for all energies and bottom two graphs demonstrate the decrease of the residuum norm for two selected energies $\epsilon_i = 2\text{eV}$ and 4eV . The different preconditioning methods are shown with different colors. The curves of the same color correspond to the two different right-hand sides $\mu_i = o, e$ in Eq. (26).

Let us first focus on graphs at the top of Fig. 6 show-

ing the performance of the GMRES method. The method converges rather well (less than 700 iterations) even without any preconditioning. The convergence is extremely fast below 2 eV (several dozens of iterations) but gets slower above this energy with maximum around 4eV. This is related to the spectrum of the anion. The electron with energy below 2 eV does not have enough energy to populate vibrational states of the anionic potential. The process of the electron scattering is therefore almost elastic, which means that the wave function is not much perturbed with respect to the initial state used for starting the iterations. Above this energy, the dynamics is much richer, which is reflected in the increased number of iterations needed to reach the converged wave function. For the most of the energies in the range of interest, the preconditioning reduces the number of iterations considerably. The least efficient preconditioning matrices M^{dg} , M^{gu} (overlapping curves in Fig. 6) include only diagonal portion of the matrix A and are therefore numerically very cheap to implement. The preconditioner M^{du} includes also terms proportional to coupling constants κ_1, κ_2 . For the ECD86 model, there are no terms in the matrix A added by increasing the size of preconditioner to M^d and M^u , the convergence curves thus overlap for these three preconditioners. The best results are obtained with the preconditioning matrix M^g which has blocks of size $2N_u \times 2N_u$ and includes terms proportional to λ in Eq. (18). The convergence of residuum norm in the lower part of Fig. 6 shows a difference in behavior of different preconditioned methods. While the best method with M^g preconditioner converges exponentially for all energies, there is kind of plateau in the other methods and the iterations without preconditioning even became more efficient at high energies.

The behavior of the COCG method (Fig. 7) is different in several aspects. The overall number of iterations is approximately three time larger (for unpreconditioned iterations) but we have to keep in mind that the COCG method is much simpler with computational demands constant over the course of the iterations. For GMRES, the computational demands for one iteration grows quadratically with the number of iterations. The COCG method does not have the minimization property (29). This is reflected in the shape of the convergence curves (two bottom graphs in Fig. 7). Unlike in similar curves for GMRES, here the residuum can locally grow although in general it finally converges to zero. The efficiency of the different preconditioning schemes is similar like in GMRES, although for higher energies only the M^g preconditioner is useful.

b. Performance of the methods for generalized model. The generalized model has a more complicated structure (23) of the level-shift operator $F(E)$, which is reflected in a more complicated structure of the matrix A , see Fig. 5. Surprisingly, the iteration methods converge faster with this matrix. There are no clear criteria relating rigorously the structure of the matrix to the speed of convergence. We believe that the faster convergence here may be re-

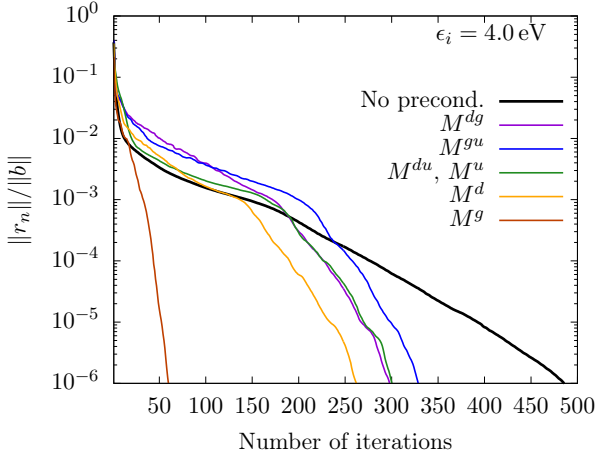
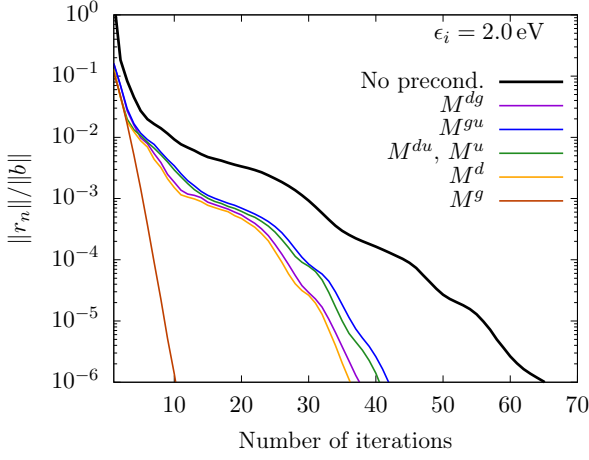
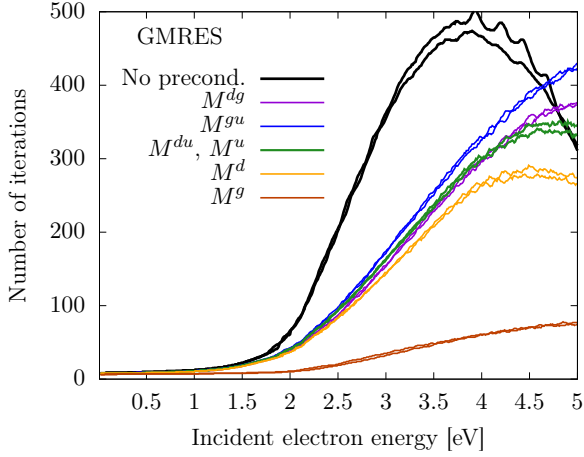


FIG. 8. Convergence of GMRES method for the generalized model, see also caption of Fig. 6 for details.

lated to the fact that operator F in generalized model increases diagonal elements of the matrix A . Apart from a little bit faster convergence, the graphs in Fig. 8 for the GMRES method in the new model look qualitatively similar as for ECD86 model. The norm of the residuum is monotonously decreasing for all methods and the preconditioner M^g is again the most efficient. The individual

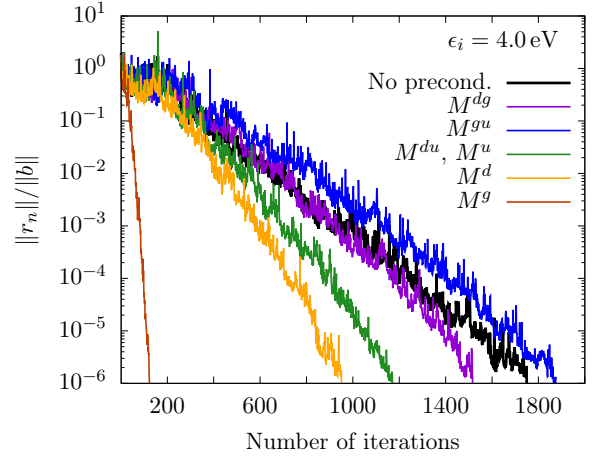
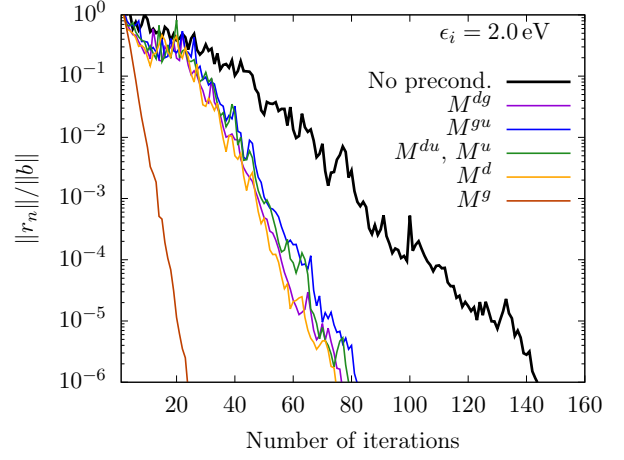
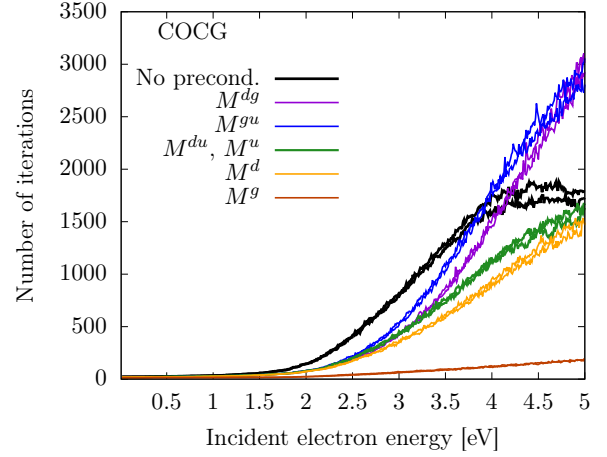


FIG. 9. Convergence of COCG method for the generalized model, see also caption of Fig. 6 for details.

preconditioners now lead to different convergence rates, because all choices of the diagonal blocks are distinct for the richer structure of A . The exception is the equivalence of M^{du} and M^u preconditioning (the green and yellow lines are overlapping in the graphs). This can be nicely understood from the structure of the matrix A depicted in Fig. 5. We see that the large and small black

diagonal boxes in the bottom right matrix differ by a blank area of zero matrix elements.

The faster convergence for the new model is even more apparent for the COCG method in Fig. 9. Now all preconditioning schemes except for M^{dg} and M^{gu} are faster than direct iterations.

To conclude the numerical experiment section, we would like to add a few notes on the implementation. Even without utilizing the structure of the matrix A , we have got by one order of magnitude faster calculation of the spectra utilizing the Krylov-subspace iteration methods as compared to a direct solver. Optimizing the matrix-vector multiplication using the structure of the matrix A explained at the beginning of Sec. III leads to the another order of magnitude speed up. From the previous examples, we see that the proper choice of preconditioning leads to the decrease of number of iterations needed for convergence by another one order of magnitude for both models and both methods.

c. Performance for model of $e^- + \text{CO}_2$. In the final part of this section, we discuss our earlier work [33–35] on the electron collisions with the carbon dioxide (CO_2) molecule in the context of the present paper. The vibronic coupling model for the $e + \text{CO}_2$ system [34] follows the general approach presented here in Sec. II C, however, the model is more complex. We considered the nuclear motion within the full four-dimensional vibrational space in combination with three electronic states ($^2\Sigma_g^+$ virtual state and two components of $^2\Pi_u$ shape resonance), which are coupled upon bending of the molecule. The Hamiltonian is thus a 3×3 matrix in the electronic space and we did not restrict its elements only to the first order in the normal coordinates (some of the elements were expanded up to the fourth order). Additionally, the three discrete states were coupled to four electron partial waves. The vibrational dynamics is described analogically to the scheme given in Sec. II D but there are four vibrational indices instead of two. The vibrational basis was constructed from products of eigenfunctions of 1D harmonic oscillators for symmetric and stretching modes and eigenfunctions of 2D harmonic oscillator expressed in polar coordinates for the two-dimensional bending mode.

Using the COCG method without any preconditioning, the number of iterations needed to reach the convergence with the stopping criterion of 10^{-3} (sufficient to obtain converged cross sections) rapidly grows with the electron energy, see Fig. 10. For energies above 3 eV, even 2×10^5 iterations were insufficient to reach the convergence, therefore, a suitable preconditioning is essential.

The slow rate of convergence or no convergence at all is caused by the coupling of the discrete states through the bending mode. The stretching modes do not affect the convergence much since we found that the COCG method converges badly even for the case where we did not consider the stretching modes.² Thus, taking a block-

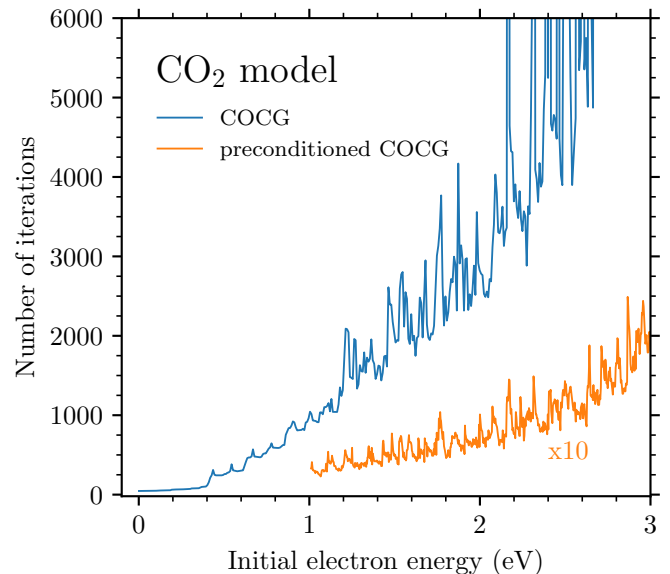


FIG. 10. Number of iterations needed to solve the Schrödinger equation for the $e + \text{CO}_2$ system using the COCG method without and with preconditioning. In the latter case, the curve is multiplied by a factor of 10.

diagonal preconditioner where blocks contain the discrete states and the two-dimensional bending was a natural choice. Such a preconditioner is analogous to the preconditioner M^g that performs the best for the ECD86 model and its generalization. In the case of CO_2 , around 200 iterations were sufficient to reach the convergence for initial electron energy of 3 eV, see Fig. 10.

IV. DISCUSSION OF RESULTING SPECTRA FOR TEST MODELS

It is not purpose of this paper to study in detail the calculated spectra and their interpretation. This will require a detailed analysis of the final-state distribution and shape of the individual components of the wave function in the coordinate representation and its relation to the shape of potentials and also study of the dependence of the results on the model parameters. It is quite voluminous work that deserves a separate paper. We would also like to identify specific molecules that can be treated with the model of the current setup or a proper generalization. We already published the generalization of the model [34] needed to describe the resulting spectra for the CO_2 molecule [33] and performed the detailed analysis [35] including the final-state distribution, the wave functions and decomposition of spectra due to contribution of components of different symmetry.

² We can easily freeze a vibrational mode by considering only the

ground state as the basis within this mode and setting all relevant model parameters to zero.

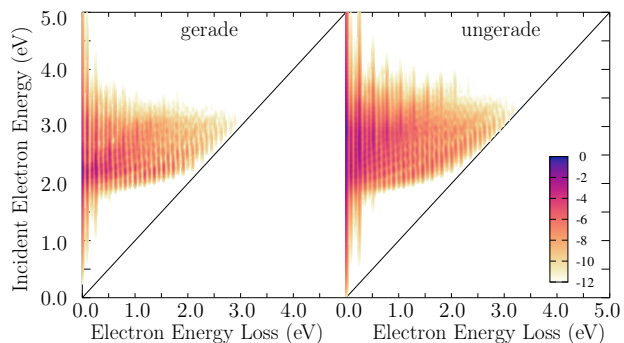
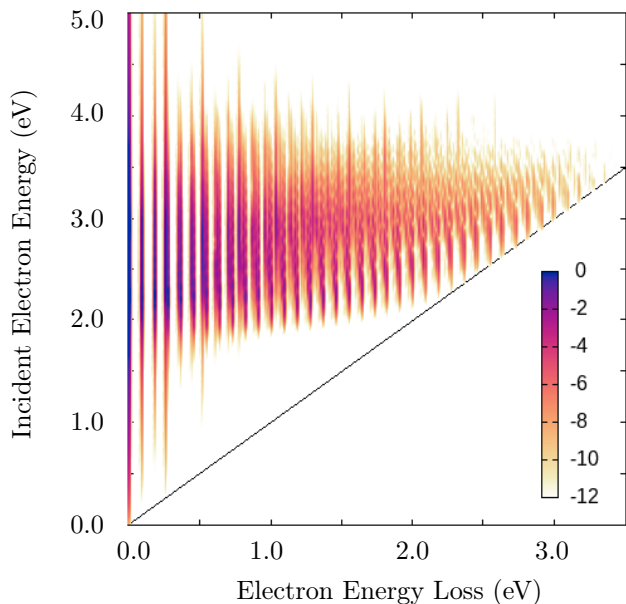


FIG. 11. 2D electron energy-loss spectrum for ECD86 model (top) and its decomposition to the gerade and ungerade symmetries (bottom). The intensity of spectrum is shown in a logarithmic scale.

In the following, we just show and briefly describe the 2D spectra for the ECD86 model (which were not subject of their original paper) and for our new generalization of the model. We also separate the contribution of the two right hand sides in Eq. (26) corresponding to the gerade and ungerade symmetry.

A. 2D spectrum for ECD86 model

The calculated 2D spectrum for the ECD86 model is shown in Fig. 11. The intensity given by Eq. (17) is plotted as a function of both energy loss $\Delta\epsilon$ and initial electron energy ϵ_i in a color logarithmic scale. It is fully converged result, i. e. it is independent of the method

used to calculate it. Interestingly enough, the spectrum is qualitatively quite similar to the 2D spectrum for the CO_2 molecule [23, 33]. The bulk of the spectrum is located at energies of the incident electron between 2-4 eV. This is a consequence of the shape of the anion potential manifold (see Figs. 1 and 2) and its location relative to the potential of the neutral molecule. The understanding of the detailed shape is not trivial. For small electron energy losses, the spectrum is discretized by vibrational frequencies whose ratio is approximately 3:1. But since this ratio is not exact, the spectrum becomes quasi-continuous for energies above 1 eV. At the same time, we see that there is some selection mechanism that singles out narrower structures close to the diagonal threshold line. There are also diagonal rays appearing in the structure of the spectrum (better apparent in the decomposition of the spectrum according to symmetries). Both of these features were present in the case of CO_2 , where we performed the detailed analysis [35].

B. 2D spectrum for new model

We proposed the new model above to consistently introduce the vibronic coupling in the level-shift operator in the ECD86 model and to test the iteration schemes to solve the dynamics in this model. The choice of the model parameters was guided by our experience with the diatomic molecules, but apart from that the choice is completely random. To our surprise, the resulting spectrum has a quite interesting intricate structure, which is furthermore similar to experimental data for some molecules, like benzene and its derivatives [56]. Particularly, we are speaking about the wedge-shaped structure with the tip touching the vertical axis at the incident electron energy of 2.2 eV, limited by this energy from below and limited approximately with the diagonal line corresponding to the electron energy loss $\Delta\epsilon = \epsilon_i + 2$ eV from above. The origin of this structure is not clear and since it is quite common in experimental data, we will dedicate the future study to this phenomenon. It indicates some selection mechanism in the dynamics that forces the system to skip through a region with small energy losses to large losses.

V. CONCLUSIONS

We derived a generalization of the model of conical intersection in electronic continuum proposed originally by Estrada et al. [32] by including terms linear in the vibrational coordinates also in the term that couples the two discrete states of the original model to two partial waves of the electronic continuum. The generalization thus produces quadratic terms in the nonlocal level-shift operator $F(E)$ that describes the dynamics of the vibrational excitation of the molecule by collision with an electron.

We also implemented two Krylov-subspace iteration

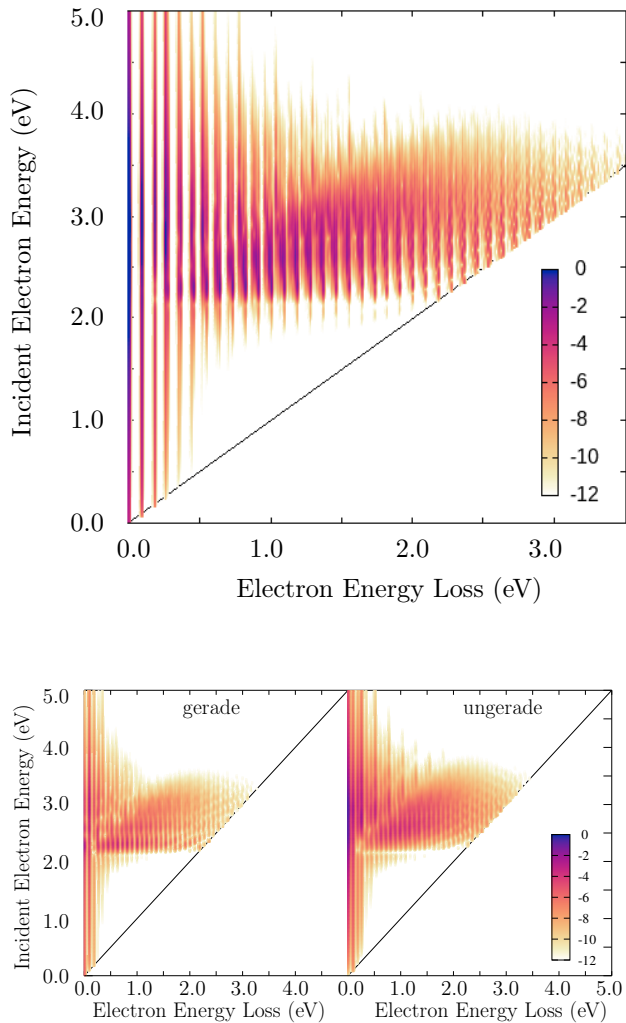


FIG. 12. The same data as in Fig. 11 but for the new model.

methods GMRES and COCG for solving the dynamics and calculation of 2D electron energy-loss spectra, and we tested the two methods on the original ECD86 model

and our generalization. The Krylov-subspace methods are ideally suited for this kind of models because the multiplication by model functions expanded in polynomials of vibrational coordinates can be implemented very efficiently in the oscillator basis. For both models we observed a very good convergence of both methods even without preconditioning. The slower convergence of the COCG method is compensated by the simplicity of its implementation. The computational demands of GMRES also grow in the course of iteration procedure. The preconditioning by block-diagonal matrix works well only for some choice of the blocks (depends on the ordering of the basis).

Out of all tested preconditioners, the M^g preconditioner proved to be the most efficient for both the two-dimensional models and our earlier realistic model of the CO_2 molecule. This seems to be a natural result since we exactly invert the blocks that involve the discrete-state space and the coupling mode. On the other hand, the most time-consuming preconditioner M^d works rather badly taken into account that we invert the blocks corresponding to the full vibrational space. Thus, the M^g preconditioner is the preconditioner of choice for more complicated models, as the one for CO_2 , where the unpreconditioned iterations are expected not to converge for all energies of interest.

We believe that the methods tested here can be used for more complicated molecules to get better understanding of the 2D electron energy-loss spectroscopy. We plan a more extensive parameter study to obtain a deeper understanding of the results. The proposed method is conceptually simple and can further be generalized in a straightforward way to include more anion states, more vibrational degrees of freedom and higher order polynomial functions. More challenging generalization will be needed to include also dissociative channels and anharmonicity in the neutral molecule.

ACKNOWLEDGMENTS

We gratefully acknowledge the financial support provided by the Czech Science Foundation Project No. 19-20524S and by the Charles University Grant Agency, Project No. 552120.

-
- [1] J. N. Bardsley and F. Mandl, Resonant scattering of electrons by molecules, Rep. Prog. Phys. **31**, 471 (1968).
 - [2] N. F. Lane, The theory of electron-molecule collisions, Rev. Mod. Phys. **52**, 29 (1980).
 - [3] M. Allan, Study of triplet-states and short-lived negative ions by means of electron-impact spectroscopy, J. Electron Spectr. Rel. Phenom. **48**, 219 (1989).
 - [4] G. J. Schulz, Resonances in electron impact on diatomic molecules, Rev. Mod. Phys. **45**, 423 (1973).
 - [5] H. Hotop, M. W. Ruf, M. Allan, and I. I. Fabrikant, Res-

- onance and threshold phenomena in low-energy electron collisions with molecules and clusters, Adv. In At. Mol. Opt. Phys. **49**, 85 (2003).
- [6] S. Ptasńska, S. Denifl, B. Mróz, M. Probst, V. Grill, E. Illenberger, P. Scheier, and T. D. Märk, Bond selective dissociative electron attachment to thymine, J. Chem. Phys. **123**, 10.1063/1.2035592 (2005).
- [7] B. C. Ibanescu and M. Allan, Selective cleavage of the C–O bonds in alcohols and asymmetric ethers by dissociative electron attachment, Phys. Chem. Chem. Phys.

- 11, 7640 (2009).
- [8] I. I. Fabrikant, S. Eden, N. J. Mason, and J. Fedor, Recent progress in dissociative electron attachment: From diatomics to biomolecules, *Adv. In At. Mol. Opt. Phys.* **66**, 545 (2017).
- [9] T. N. Rescigno, W. A. Isaacs, A. E. Orel, H.-D. Meyer, and C. W. McCurdy, Theoretical study of resonant vibrational excitation of CO₂ by electron impact, *Phys. Rev. A* **65**, 032716 (2002).
- [10] C. W. McCurdy, W. A. Isaacs, H.-D. Meyer, and T. N. Rescigno, Resonant vibrational excitation of CO₂ by electron impact: Nuclear dynamics on the coupled components of the ²Π_u resonance, *Phys. Rev. A* **67**, 042708 (2003).
- [11] T. N. Rescigno, C. S. Trevisan, and A. E. Orel, Dynamics of low-energy electron attachment to formic acid, *Phys. Rev. Lett* **96**, 213201 (2006).
- [12] G. A. Gallup, P. D. Burrow, and I. I. Fabrikant, Electron-induced bond breaking at low energies in HCOOH and glycine: The role of very short-lived σ* anion states, *Phys. Rev. A* **79**, 042701 (2009).
- [13] R. Čurík, P. Čárský, and M. Allan, Vibrational excitation of methane by slow electrons revisited: theoretical and experimental study, *J. Phys. B: At., Mol. Opt. Phys.* **41**, 115203 (2008).
- [14] R. Čurík, I. Paidarová, M. Allan, and P. Čárský, Joint experimental and theoretical study on vibrational excitation cross sections for electron collisions with diacetylene, *J. Phys. Chem. A* **118**, 9734 (2014).
- [15] P. Nag, R. Čurík, M. Tarana, M. Polášek, M. Ehara, T. Sommerfeld, and J. Fedor, Resonant states in cyanogen NCCN, *Phys. Chem. Chem. Phys.* **22**, 23141 (2020).
- [16] C. S. Anstöter, G. Mensa-Bonsu, P. Nag, M. Ranković, R. Kumar T. P., A. N. Boichenko, A. V. Bochenkova, J. Fedor, and J. R. R. Verlet, Mode-specific vibrational autodetachment following excitation of electronic resonances by electrons and photons, *Phys. Rev. Lett.* **124**, 203401 (2020).
- [17] G. A. Gallup, Selection rules for vibrational energy loss by resonant electron impact in polyatomic molecules, *Phys. Rev. A* **34**, 2746 (1986).
- [18] G. A. Gallup, Symmetry selection rules for vibrational excitation by resonant electron impact and a unified treatment of vibronic coupling between resonances and to the continuum: A complete symmetry analysis of vibrational excitation in benzene, *J. Chem. Phys.* **99**, 827 (1993).
- [19] R. Čurík, P. Čárský, and M. Allan, Electron-impact vibrational excitation of cyclopropane, *J. Chem. Phys.* **142**, 144312 (2015).
- [20] R. Marion, M. Čížek, and X. Urbain, Autodetachment spectroscopy of metastable D₂⁻ and HD⁻, *Phys. Rev. A* **107**, 052808 (2023).
- [21] M. Ranković, P. Nag, C. S. Anstöter, G. Mensa-Bonsu, R. Kumar T. P., J. R. R. Verlet, and J. Fedor, Resonances in nitrobenzene probed by the electron attachment to neutral and by the photodetachment from anion, *J. Chem. Phys.* **157**, 064302 (2022).
- [22] T. Reddish, F. Currell, and J. Comer, Studies of the 2 eV shape resonance in N₂ using a two-dimensional scanning technique, *J. Phys. E: Sci. Instrum.* **21**, 203 (1988).
- [23] F. Currell and J. Comer, *Phys. Rev. Lett.* **74**, 1319 (1995).
- [24] K. Regeta and M. Allan, Autodetachment dynamics of acrylonitrile anion revealed by two-dimensional electron impact spectra, *Phys. Rev. Lett.* **110**, 203201 (2013).
- [25] K. Regeta and M. Allan, Two-dimensional spectra of electron collisions with acrylonitrile and methacrylonitrile reveal nuclear dynamics, *J. Chem. Phys.* **142**, 184307 (2015).
- [26] M. Allan, K. Regeta, J. D. Gorfinkiel, Z. Mašín, S. Grimme, and C. Bannwarth, Recent research directions in Fribourg: nuclear dynamics in resonances revealed by 2-dimensional EEL spectra, electron collisions with ionic liquids and electronic excitation of pyrimidine, *Eur. Phys. J. D* **70**, 123 (2016).
- [27] M. Allan, M. Lacko, P. Papp, Š. Matejčík, M. Zlatar, I. I. Fabrikant, J. Kočíšek, and J. Fedor, Dissociative electron attachment and electronic excitation in Fe(CO)₅, *Phys. Chem. Chem. Phys.* **20**, 11692 (2018).
- [28] M. Ranković, P. Nag, M. Zawadzki, L. Ballauf, J. Žabka, M. Polášek, J. Kočíšek, and J. Fedor, Electron collisions with cyanoacetylene HC₃N: Vibrational excitation and dissociative electron attachment, *Phys. Rev. A* **98**, 052708 (2018).
- [29] M. Ranković, R. Kumar T P, P. Nag, J. Kočíšek, and J. Fedor, Temporary anions of the dielectric gas C₃F₇CN and their decay channels, *J. Chem. Phys.* **152**, 244304 (2020).
- [30] J. Med, Š. Sršeň, P. Slavíček, A. Domaracka, S. Indrajith, P. Rousseau, M. Fárník, J. Fedor, and J. Kočíšek, Vibrationally mediated stabilization of electrons in nonpolar matter, *J. Phys. Chem. Lett.* **11**, 2482 (2020).
- [31] R. Kumar T. P., J. Kočíšek, K. Bravaya, and J. Fedor, Electron-induced vibrational excitation and dissociative electron attachment in methyl formate, *Phys. Chem. Chem. Phys.* **22**, 518 (2020).
- [32] H. Estrada, L. S. Cederbaum, and W. Domcke, Vibronic coupling of short-lived electronic states, *J. Chem. Phys.* **84**, 152 (1986).
- [33] J. Dvořák, M. Ranković, K. Houfek, P. Nag, R. Čurík, J. Fedor, and M. Čížek, Vibronic coupling through the continuum in the e + CO₂ system, *Phys. Rev. Lett.* **129**, 013401 (2022).
- [34] J. Dvořák, K. Houfek, and M. Čížek, Vibrational excitation in the e + CO₂ system: Nonlocal model of ΣΠ vibronic coupling through the continuum, *Phys. Rev. A* **105**, 062821 (2022).
- [35] J. Dvořák, M. Ranković, K. Houfek, P. Nag, R. Čurík, J. Fedor, and M. Čížek, Vibrational excitation in the e + CO₂ system: Analysis of two-dimensional energy-loss spectrum, *Phys. Rev. A* **106**, 062807 (2022).
- [36] F. A. Gianturco and A. Jain, The theory of electron scattering from polyatomic molecules, *Phys. Rep.* **143**, 347 (1986).
- [37] W. Domcke, Theory of resonance and threshold effects in electron-molecule collisions: The projection-operator approach, *Phys. Rep.* **208**, 97 (1991).
- [38] M. Čížek and K. Houfek, Nonlocal Theory of Resonance Electron-Molecule Scattering, in *Low-energy Electron Scattering from Molecules, Biomolecules and Surfaces*, edited by P. Čárský and R. Čurík (CRC Press, 2012) Chap. 4, pp. 91–125.
- [39] L. H. Scarlett, I. Bray, and V. D. Fursa, Electronic and vibrational close-coupling method for resonant electron-molecule scattering, *Phys. Rev. Lett.* **127**, 223401 (2021).
- [40] R. Čurík and P. Čárský, Vibrationally inelastic electron

- scattering on polyatomic molecules by the discrete momentum representation (DMR) method, *J. Phys. B* **36**, 2165 (2003).
- [41] F. Kossoski and B. Mario, Nonadiabatic dynamics in multidimensional complex potential energy surfaces, *Chem. Sci.* **11**, 9827 (2020).
- [42] H. B. Ambalampitiya and I. I. Fabrikant, Nonlocal complex potential theory of dissociative electron attachment: Inclusion of two vibrational modes, *Phys. Rev. A* **102**, 022802 (2020).
- [43] S. Feuerbacher, T. Sommerfeld, and L. S. Cederbaum, Intersections of potential energy surfaces of short-lived states: The complex analogue of conical intersections, *J. Chem. Phys.* **120**, 3201 (2004).
- [44] S. Feuerbacher and L. S. Cederbaum, Jahn-Teller effect for short-lived states: Study of the complex potential energy surfaces, *J. Chem. Phys.* **121**, 5 (2004).
- [45] H. Feshbach, A unified theory of nuclear reactions II, *Ann. Phys.* **19**, 287 (1962).
- [46] F. H. Mies, Configuration interaction theory. Effect of overlapping resonances, *Phys. Rev.* **175**, 164 (1968).
- [47] M. Berman, H. Estrada, L. S. Cederbaum, and W. Domcke, Nuclear dynamics in resonant electron-molecule scattering beyond the local approximation: The 2.3-eV shape resonance in N_2 , *Phys. Rev. A* **28**, 1363 (1983).
- [48] T. P. Ragesh Kumar, P. Nag, M. Ranković, T. F. M. Luxford, J. Kočišek, Z. Mašín, and J. Fedor, Distant symmetry control in electron-induced bond cleavage, *J. Phys. Chem. Lett.* **13**, 11136 (2022).
- [49] Y. Saad and M. H. Schultz, GMRES: A generalized minimal residual algorithm for solving nonsymmetric linear systems, *SIAM J. on Scientific & Statistical Computing* **7**, 856 (1986).
- [50] V. Faber and T. Manteuffel, Necessary and sufficient conditions for the existence of a conjugate gradient method, *SIAM J. on Num. Analysis* **21**, 352 (1984).
- [51] J. Liesen and Z. Strakoš, *Krylov subspace methods : principles and analysis* (Oxford University Press, 2013).
- [52] H. A. van der Vorst and J. Melissen, A Petrov-Galerkin type method for solving $Ax=b$, where A is symmetric complex, *IEEE Transactions on Magnetics* **26**, 706 (1990).
- [53] Y. Saad, *Iterative methods for sparse linear systems* (Society for Industrial and Applied Mathematics, 2003).
- [54] M. Šarmanová, *Iterative calculation of vibrational dynamics in electron scattering from molecule*, Bcl thesis, Charles University, Prague, <http://hdl.handle.net/20.500.11956/121270> (2020).
- [55] M. Šarmanová, *Mathematical modeling of vibrational dynamics in electron scattering from molecule*, Ms thesis, Charles University, Prague, <http://hdl.handle.net/20.500.11956/175327> (2022).
- [56] M. Allan, Two-dimensional electron-energy loss spectra reveal nuclear dynamics of negative ion resonances. (2019), Talk, Telluride, <https://homeweb.unifr.ch/allanm/pub/ma/Lectures.html> (unpublished).